nature genetics

Altered brain microRNA biogenesis contributes to phenotypic deficits in a 22q11-deletion mouse model

Kimberly L Stark[1,6], Bin Xu[2,6], Anindya Bagchi[3], Wen-Sung Lai[2], Hui Liu[1], Ruby Hsu[4], Xiang Wan[5], Paul Pavlidis[5], Alea A Mills[3], Maria Karayiorgou[1] & Joseph A Gogos[2,4]

Individuals with 22q11.2 microdeletions show behavioral and cognitive deficits and are at high risk of developing schizophrenia. We analyzed an engineered mouse strain carrying a chromosomal deficiency spanning a segment syntenic to the human 22q11.2 locus. We uncovered a previously unknown alteration in the biogenesis of microRNAs (miRNAs) and identified a subset of brain miRNAs affected by the microdeletion. We provide evidence that the abnormal miRNA biogenesis emerges because of haploinsufficiency of the *Dgcr8* gene, which encodes an RNA-binding moiety of the 'microprocessor' complex and contributes to the behavioral and neuronal deficits associated with the 22q11.2 microdeletion.

Hemizygous microdeletions of the 22q11.2 locus are among the most common chromosomal abnormalities[1] and occur predominantly (~90%) *de novo*[2]. Although some variability in the breakpoints exists, most microdeletions (~87%) are 3 Mb in size[3]. A smaller percentage of them (~8%) involve the same proximal but a different distal breakpoint, resulting in a smaller, 1.5-Mb deletion[3] (**Supplementary Fig. 1** online). Children with the 22q11.2 microdeletion show increased incidence of emotional problems, such as anxiety, depression and social withdrawal[4], as well as childhood pathologies such as attention-deficit hyperactivity disorder, obsessive-compulsive disorder and autism spectrum disorders[5–7]. Individuals with the 22q11.2 microdeletion also show a spectrum of deficits in cognitive tasks linked to activity in prefrontal cortex (PFC) and hippocampus, such as measures of attention, working memory, executive function and short-term verbal memory[4,8,9]. Approximately 30% of them develop typical schizophrenia or schizoaffective disorder in adolescence or early adulthood[10]. Microdeletions of 22q11.2 account for up to 1–2% of schizophrenia cases[11] and represent the only known recurrent copy number mutation responsible for introducing new cases of schizophrenia in the population.

Genetic studies in humans, augmented by analysis of reliable animal models, have identified a small subset of the deleted genes and their interactions as contributing to the 22q11-associated psychiatric phenotypes[12–18]. Further studies in animal models have focused primarily on abnormalities of prepulse inhibition (PPI)[19], a measure of preattentive processing and a nonspecific endophenotype of several psychiatric and neurological disorders, and have identified several genes from this region that modulate PPI[16,20–22]. However, with a few exceptions[16], the genetic basis of the cognitive deficits associated with this syndrome is still largely unexplored.

In the present study, we analyzed an engineered mouse strain carrying a hemizygous chromosomal deficiency on mouse chromosome 16 that spans a segment syntenic to the 1.5-Mb 22q11.2 microdeletion[3]. We uncovered alterations in the biogenesis of brain miRNAs, a class of small, noncoding RNAs that in animals regulate gene expression (primarily by inhibiting mRNA translation or stability) and found that abnormal miRNA biogenesis was due to haploinsufficiency of the *Dgcr8* gene, which is included in the chromosomal deficiency and contributed to the behavioral and neuronal deficits induced by this chromosomal deficiency.

RESULTS

Df(16)A$^{+/-}$ mice show behavioral and cognitive deficits

Using chromosomal engineering[23–25], we generated a mouse model carrying a hemizygous 1.3-Mb chromosomal deficiency (*Df(16)A*$^{+/-}$), ranging from *Dgcr2* to *Hira* (**Supplementary Fig. 1**), that spans a segment syntenic to the 1.5-Mb human 22q11.2 microdeletion and encompasses 27 genes. Almost all of the functional genes in the human segment are represented in the mouse segment, organized in a slightly different order. *Df(16)A*$^{+/-}$ mice did not show any gross anatomical brain abnormalities (data not shown), but they showed deficits in synaptic connectivity in the hippocampus that included a reduction in the number and size of dendritic spines, as well

[1]Department of Psychiatry, College of Physicians and Surgeons, Columbia University, 1051 Riverside Drive, New York, New York 10032, USA. [2]Department of Physiology and Cellular Biophysics, College of Physicians and Surgeons, Columbia University, 630 West 168th Street, New York, New York 10032, USA. [3]Cold Spring Harbor Laboratory, 1 Bungtown Road, Cold Spring Harbor, New York 11724, USA. [4]Department of Neuroscience, College of Physicians and Surgeons, Columbia University, 1051 Riverside Drive, New York, New York 10032, USA. [5]Department of Psychiatry and Bioinformatics Centre, University of British Columbia, 2185 East Mall, Vancouver, British Columbia V6T 1Z4, Canada. [6]These authors contributed equally to this work. Correspondence should be addressed to M.K. (mk2758@columbia.edu) or J.A.G. (jag90@columbia.edu).

Received 10 December 2007; accepted 13 March 2008; published online 11 May 2008; doi:10.1038/ng.138

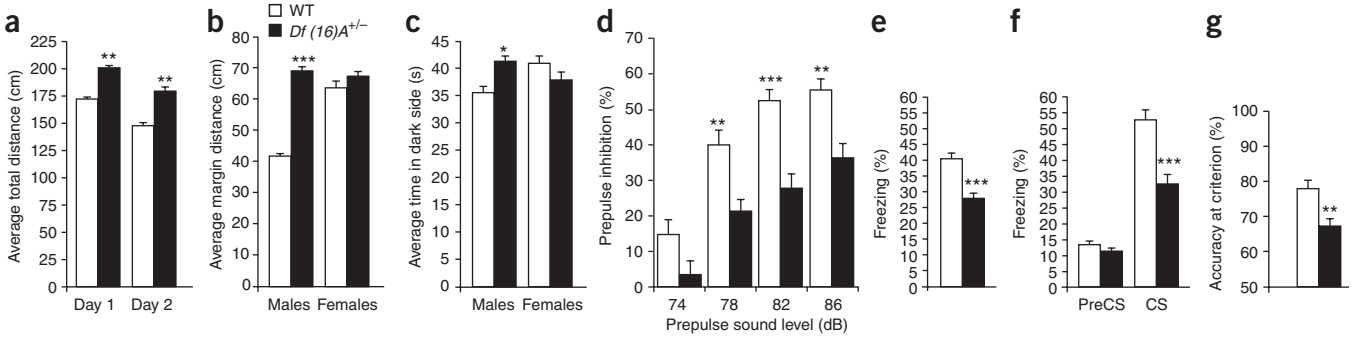

Figure 1 *Df(16)A*$^{+/-}$ mice are hyperactive and show deficits in sensorimotor gating and two learning tasks. (**a**) Activity of *Df(16)A*$^{+/-}$ and WT littermate control mice in the open field on two consecutive days. In both a 1-h exposure to a novel open field (day 1) and a 30-min reexposure 24 h later (day 2), *Df(16)A*$^{+/-}$ mice were consistently hyperactive. (**b**) Total distance traveled in the margin of the open field was significantly different between male (but not female) *Df(16)A*$^{+/-}$ mice and WT mice. (**c**) In a light–dark transition test, male *Df(16)A*$^{+/-}$ mice spent significantly more time in the dark than male WT mice. There was no difference between genotypes in the females. (**d**) *Df(16)A*$^{+/-}$ mice (pooled data from males and females) showed impaired sensorimotor gating as assayed by the PPI test. Percent PPI was calculated as 100 – [(startle response of acoustic startle from acoustic prepulse and startle stimulus trials/startle response alone trials) × 100]. (**e**,**f**) Fear conditioning test. Twenty-four hours after exposure to the tone and foot-shock pairings, *Df(16)A*$^{+/-}$ mice froze less than WT mice when placed in the same context (**e**). Two hours after exposure to the contextual chamber, mice were placed into a novel chamber (PreCS), and no significant differences were found in freezing between genotypes (**f**). When presented with the tone (CS), *Df(16)A*$^{+/-}$ mice froze significantly less than WT mice (**f**). (**g**) Spatial working memory–dependent learning test. *Df(16)A*$^{+/-}$ mice showed learning deficits in arm choice accuracy during test acquisition. The vertical axis starts at 50% correct responses, which represents baseline accuracy expected by chance. Criterion, the average choice accuracy during a training period, where the training endpoint was defined as two consecutive days of 70% choice accuracy or greater. $^{*}P < 0.05$, $^{**}P < 0.01$, $^{***}P < 0.001$. Data are presented as mean ± s.e.m.

as a decrease in dendritic complexity of CA1 pyramidal neurons (J. Mukai, A. Dhilla, L.J. Drew, K.L.S., L. Cao, *et al.*, unpublished data).

To analyze the consequences of *Df(16)A* on behavior, we first evaluated the general response of *Df(16)A*$^{+/-}$ mice to a novel open-field environment. We found the *Df(16)A*$^{+/-}$ mice to be hyperactive compared to wild-type (WT) littermates, as shown by an increase in total path length traveled over a 1-h exposure period (**Fig. 1a**, day 1). There was a significant main effect of genotype ($P < 0.01$) and no significant genotype × sex interaction ($P > 0.05$). On a subsequent 30-min reexposure 24 h later, *Df(16)A*$^{+/-}$ mice remained hyperactive (**Fig. 1a**, day 2). By comparing center to margin measures (an index of fear response), we found that there was a significant effect of genotype on margin distance ($P < 0.0001$), as well as a significant sex × genotype interaction ($P < 0.001$). By considering the sexes separately, we found that male but not female *Df(16)A*$^{+/-}$ mice traveled more in the margins ($P < 0.0001$, **Fig. 1b**) and less in the aversive center of the open field ($P = 0.06$; data not shown), an indication that they were more fearful of exploring the novel environment. To further characterize this response, we tested a separate group of mice in the light–dark transition test and confirmed that male *Df(16)A*$^{+/-}$ mice spent longer on the dark side than did their WT counterparts ($P < 0.05$, **Fig. 1c**).

Animal models carrying large deficiencies at loci syntenic to human 22q11 have consistently shown abnormalities in sensorimotor gating, as assayed by the PPI test, although the pattern of alterations differs somewhat among studies[22,26,27]. Alterations in sensorimotor gating seem to be the result of an interplay between both positive[22] and negative[21] contributions from genes residing in this locus. Consistent with previous studies, we found that both male and female *Df(16)A*$^{+/-}$ mice showed deficits in the PPI task (**Fig. 1d**, pooled data from both sexes). In control experiments, we showed that there were no genotypic differences in either sex in the amplitude of the startle response at 120 dB (data not shown), indicating unaffected integrity and excitability of the responding neurons in subcortical auditory centers.

In order to evaluate cognitive ability, we first used the pavlovian conditioned-fear protocol to assess associative learning and memory in *Df(16)A*$^{+/-}$ mice. In the contextual fear-conditioning test, which is both amygdala and hippocampus dependent[28], *Df(16)A*$^{+/-}$ mice froze significantly less than did WT mice when they were returned to the context in which they had received the shock 24 h after training (**Fig. 1e**) ($P < 0.001$). We found no significant genotype × sex interaction for this measure, and both sexes were equally affected. In the cued version of the test, which requires the amygdala but not the hippocampus[28], tone-dependent freezing was also significantly reduced in *Df(16)A*$^{+/-}$ mice (**Fig. 1f**) ($P < 0.0001$). We found no significant interaction of sex × genotype, and both sexes were equally affected (see also **Supplementary Note** and **Supplementary Fig. 2** online).

We also examined whether spatial working memory–dependent learning[16,29] was affected in *Df(16)A*$^{+/-}$ mice. Mice were trained, using a short memory-retention interval, to enter the appropriate arm of a T-maze in order to obtain a food reward whose location was alternated on each trial. Acquisition of this task is dependent on the integrity of fronto-hippocampal circuitry[30,31]. *Df(16)A*$^{+/-}$ mice showed decreased arm choice accuracy ($P < 0.01$) over the course of the acquisition period (**Fig. 1g**). We found no significant genotype × sex interaction for this measure.

Df(16)A$^{+/-}$ mice show brain transcriptome alterations

To identify affected biological processes and molecular functions[16], we resorted to an unbiased evaluation of the transcriptional responses in the hippocampus and PFC of the *Df(16)A*$^{+/-}$ mice. Analysis of GeneChip data identified 2,521 probe sets (5.6%, ~2,087 unique transcripts) in PFC and 455 probe sets (1%, ~455 unique transcripts in hippocampus as being differentially expressed with false-discovery rate (FDR)-corrected *t*-test *P*-values < 0.05. At a more stringent FDR of 0.01, we found 837 probe sets (1.9%, ~716 transcripts) in PFC and 96 probe sets (0.21%, ~83 transcripts) in hippocampus as being differentially expressed. We observed the expected downregulation of

all genes within the deficiency (FDR *P*-values: in PFC, $P = 10^{-2}$ to 10^{-12}, $n = 20$; in hippocampus, $P = 10^{-2}$ to 10^{-10}, $n = 20$) (**Fig. 2a,b** (yellow dots) and **Supplementary Table 1** online). A comparison of our results with other expression profiling studies of this locus[32–34] is provided in the **Supplementary Note**.

The number of differentially expressed probe sets outside the deficiency shared between PFC and hippocampus is 136 (at FDR *P*-value < 0.05) or 18 (at a more stringent FDR *P*-value < 0.01; see **Supplementary Table 2** online). This partial overlap was confirmed by gene-class testing based on Gene Ontology terms (see **Supplementary Methods** online). Notably, for the PFC data, altered biological processes and molecular functions contained terms that were associated with oxidative phosphorylation, oxidoreductase and active transport activities, and the cellular component terms were associated with mitochondria (**Fig. 2c** and data not shown). This pattern of change could indicate a lower rate of energy expenditure in the PFC of the mutant mice that could be directly related to inadequate expression of the mitochondrial genes located within the deleted region, such as *Slc25a1*, *Txnrd2* and *Mrpl40*, as well as *Prodh*. Alternatively, it may reflect compensatory phenomena that dynamically adjust for an underlying increase in energy expenditure at PFC. In contrast, for the hippocampal data, significantly altered biological processes and molecular functions centered on synaptic transmission and on regulation of neurotransmitter levels and binding, including changes in a cluster of gene products that interact functionally and physically with DLG4 (PSD95), an adaptor molecule implicated in glutamatergic signaling. Cellular component terms were associated with synapses and coated vesicles (**Fig. 2d,e** and data not shown).

Expression changes shared between the two brain regions may provide clues to the nature of key signaling pathways affected. Inspection of the 'stringent' list of genes shared between the PFC and the hippocampus (FDR *P*-value < 0.01) showed several known genes (see **Supplementary Note**). Notably, 6 of the 18 probe sets in this list were located in the immediate vicinity of genes containing miRNAs (**Fig. 2a,b** (blue dots) and **Supplementary Table 2**), including the *Mirg* gene, a noncoding RNA gene that is highly expressed in the adult brain and contains the largest miRNA cluster in the mouse genome[35]. Further analysis (see Methods), identified 16 more probe sets (corresponding to 9 different transcripts) that showed significant changes in expression in the PFC of *Df(16)A*$^{+/-}$ mice (see **Supplementary Table 3** online). Notably, these probe sets were invariably upregulated. Because of nonoptimal distribution of probe sets relative to miRNA genes, analysis of GeneChip data cannot offer a comprehensive view of the changes in miRNA expression. However, the observation that probe sets overlapping with known miRNA locations are among the top-scoring ones (**Fig. 2a,b**) highlights the relative importance of these changes in the context of the entire transcriptome.

Df(16)A$^{+/-}$ mice show brain miRNA biogenesis alterations

We speculated that the consistent upregulation of miRNA-related transcripts might reflect, at least in part, the upregulation of the primary forms (pri-forms) of miRNAs because one of the genes disrupted by Df(16)A, *Dgcr8*, encodes a double-stranded RNA binding protein and an important component of the 'microprocessor' complex that processes pri-forms to mature miRNAs (reviewed in ref. 36).

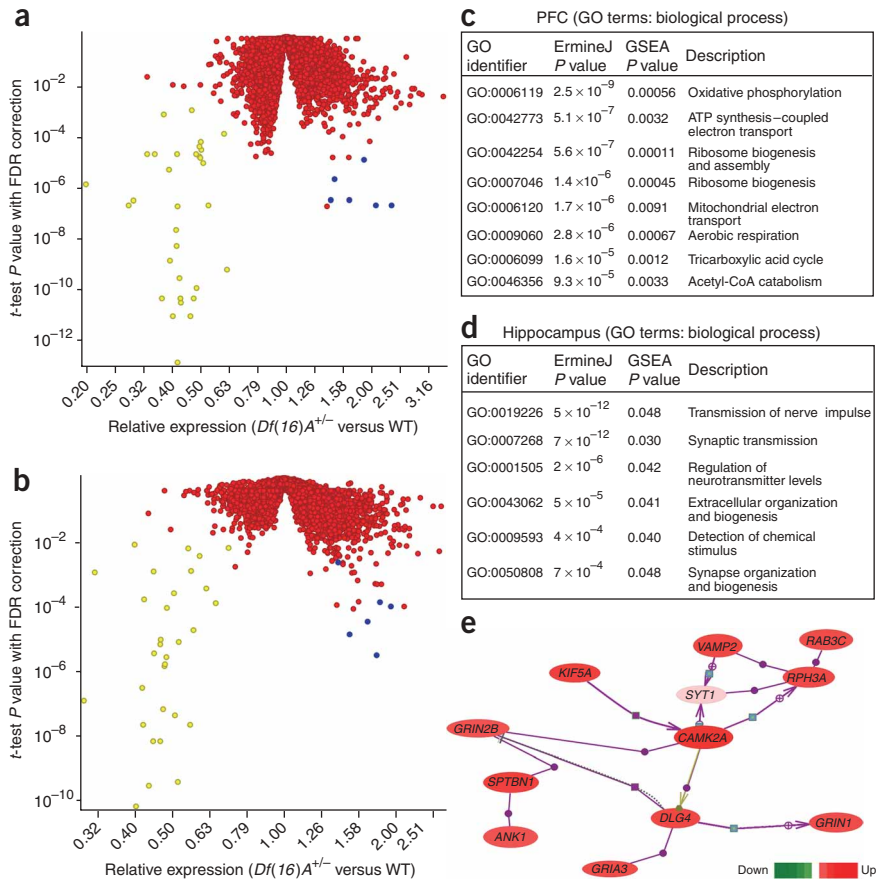

Figure 2 Transcriptome alterations in the PFC and hippocampus of *Df(16)A*$^{+/-}$ mice. (**a**,**b**) Changes in gene expression in the PFC (**a**) or hippocampus (**b**) of *Df(16)A*$^{+/-}$ and WT littermate control mice: Volcano plot of the FDR *P*-values and the corresponding relative expression of each gene. The FDR *P*-values for differences in gene expression were calculated using *t*-tests and plotted as log(*P*). Yellow dots, genes within *Df(16)A* deficiency; blue dots, changes in miRNA-containing transcripts shared between PFC and hippocampus; red dots, remainder of probe sets. (**c**,**d**) Gene Ontology (GO) terms (biological processes) that demonstrated significant alterations in PFC (**c**) or hippocampus (**d**), based on both ErmineJ analysis and Gene Set Enrichment Analysis (GSEA). (**e**) An affected multinodal gene interaction network identified in the hippocampus of *Df(16)A*$^{+/-}$ mice driven by a set of well established functional interactions of *Dlg4* (*Psd95*) at glutamatergic synapses. *Ank1*, ankyrin 1; *Camk2a*, calcium/calmodulin-dependent protein kinase II alpha; *Dlg4*, discs-large homolog 4; *Gria3*, glutamate receptor, ionotropic, AMPA 3; *Grin1*, glutamate receptor, ionotropic, *N*-methyl-D-aspartate 1; *Grin2b*, glutamate receptor, ionotropic, *N*-methyl-D-aspartate 2B; *Kif5a*, kinesin family member 5A; *Rab3c*, member 3C of RAS oncogene family; *Rph3a*, rabphilin 3A; *Spnb2*, spectrin, beta, nonerythrocytic 1; *Syt1*, synaptotagmin I; *Vamp2*, vesicle-associated membrane protein 2. Color of oval indicates upregulation (up) or downregulation (down) of relative expression in *Df(16)A*$^{+/-}$ mice. Solid line with arrow, positive regulation; bar across line, negative regulation; circle, binding; square, regulation; cross, protein modification; purple line, protein-protein interaction; green line, protein modification; dotted line, chemical reaction.

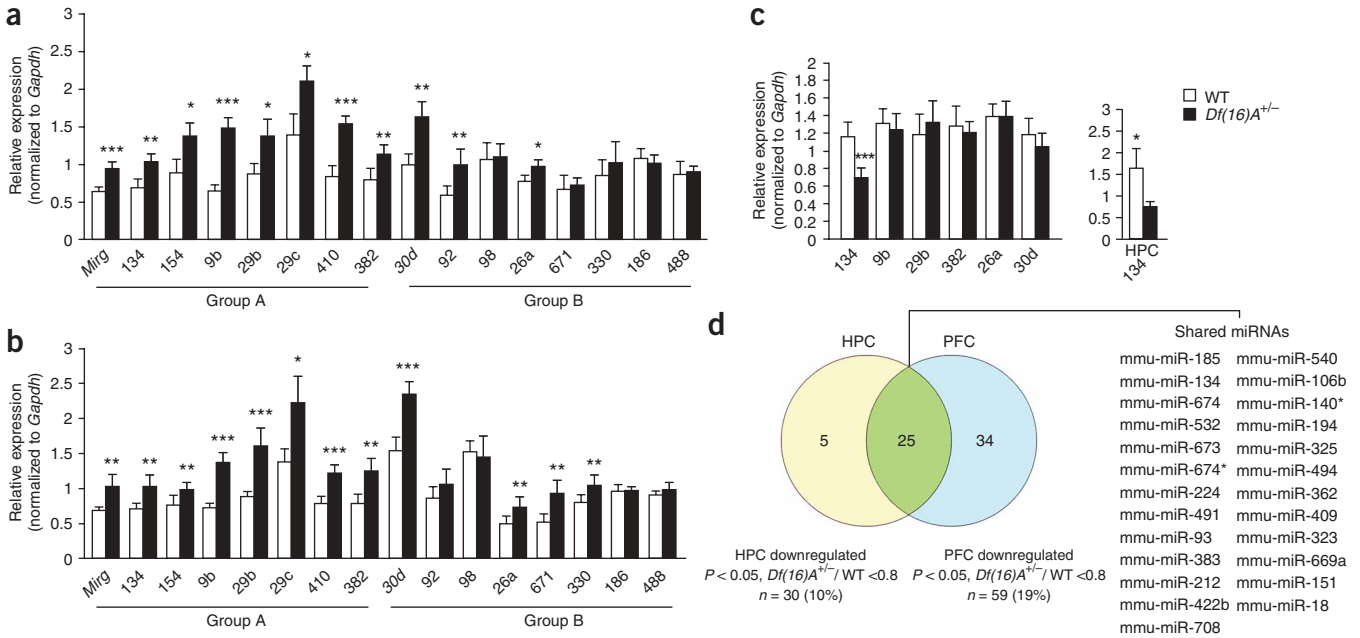

Figure 3 miRNA biogenesis alterations in the PFC and hippocampus (HPC) of *Df(16)A*$^{+/-}$ mice. (**a**,**b**) Expression of 15 miRNA pri-forms in the PFC (**a**) or hippocampus (**b**) of *Df(16)A*$^{+/-}$ and WT littermate control mice, as assayed by qRT-PCR. Group A, miRNAs in the vicinity of differentially upregulated probe sets. Group B, miRNAs in the vicinity of nondifferentially expressed probe sets. (**c**) Left, expression of six miRNA mature forms in the PFC of *Df(16)A*$^{+/-}$ mice and WT littermate controls, as assayed by qRT-PCR. Right, expression of mir-134 mature form in hippocampus of *Df(16)A*$^{+/-}$ and WT littermate controls, as assayed by qRT-PCR. In **a**–**c**, $^{*}P < 0.05$, $^{**}P < 0.01$, $^{***}P < 0.001$. Data are presented as mean ± s.e.m. (**d**) Left, Venn diagram summarizing the pattern of downregulation of miRNAs in PFC and hippocampus of *Df(16)A*$^{+/-}$ mice. Right, list of the downregulated miRNAs shared between PFC and hippocampus of *Df(16)A*$^{+/-}$ mice. Mmu, *Mus musculus*. Asterisk indicates the less predominant mature form when miRNA hairpin precursors give rise to two excised miRNAs, one from each arm.

Quantitative RT-PCR (qRT-PCR) in *Df(16)A*$^{+/-}$ mice confirmed that *Dgcr8* abundance was decreased to 57% in PFC (*t*-test, $P = 0.006$) (**Supplementary Fig. 3** online) and to 64% in hippocampus (*t*-test, $P = 0.002$) (data not shown) compared to that in WT mice.

Dgcr8 deficiency would be expected to impose a 'bottleneck' in miRNA processing. To confirm this and characterize in more detail the effect that haploinsufficiency of the *Dgcr8* gene has on brain miRNA biogenesis, we first performed pri-form–specific qRT-PCR on a group of 15 miRNA genes, using an independent set of mice. We selected, on the basis of our microarray data, seven of these genes as being in the vicinity of probe sets differentially upregulated in the PFC and hippocampus (**Fig. 3a**,**b**, group A). The rest ($n = 8$) were in the vicinity of nondifferentially expressed probe sets and were selected solely on the basis of available brain expression data[37] (**Fig. 3a**,**b**, group B). Our qRT-PCR results matched the microarray data well, as the *Mirg* gene and six out of six pri-forms selected on the basis of this data showed upregulation in both PFC and hippocampus (**Fig. 3a**,**b**). In addition, three of the eight additional pri-forms also showed upregulation in the PFC and four out of eight showed upregulation in the hippocampus, albeit in a partially overlapping pattern. Thus, overall, our results indicated upregulation of a subset of pri-miRNA forms in the PFC and hippocampus of *Df(16)A*$^{+/-}$ mice. We also examined the expression of six mature miRNA forms whose corresponding pri-forms had been tested and found to be upregulated. Only in one out of six cases was the increase in pri-miRNA accompanied by a decrease in mature form. Specifically, mir-134 showed a 40% decrease in PFC ($P = 0.0003$) and a 54% decrease in hippocampus ($P = 0.039$) (**Fig. 3c**). The observation of normal mature miRNA abundances in the presence of increased pri-form amounts could be, in part, due to the emergence of *in vivo* compensation at some later step in the miRNA biogenesis pathway. To begin addressing this issue, we looked for transcriptional upregulation of four other key genes in this pathway (*Rnasen* (*Drosha*), *Eif2c2* (*Ago2*), *Dicer1* and *Xpo5* (Exportin 5))[38] using qRT-PCR, but we did not find any changes in mRNA levels (see **Supplementary Fig. 3**).

To obtain a more comprehensive view of the number and identity of mature miRNAs that are downregulated in response to the microdeletion, we compared the expression of 386 known mature mouse miRNAs in the PFC and hippocampus of *Df(16)A*$^{+/-}$ mice and WT littermates using an miRNA microarray-based assay (see Methods). To minimize hybridization interference from upregulated pri-forms, total RNA was size-fractionated (<300 nucleotides) before hybridization (see Methods). We used for further analysis 297 miRNAs that showed positive signals above the mean background for all replicated spots on the array. We identified 59 miRNAs (~19%) in PFC and 30 (~10%) in hippocampus that showed significant downregulation (ratio *Df(16)A*$^{+/-}$/WT < 0.8, FDR *P*-value < 0.05) (**Fig. 3d** and **Supplementary Table 4** online). Notably, among them, 25 miRNAs were shared between PFC and hippocampus (**Fig. 3d** and **Table 1**). Initial validation of our approach was offered by the identification of mir-185 (located within the microdeletion) as the top-scoring miRNA, as well as by the identification of mir-134 among the top-five scoring miRNAs in both PFC and hippocampus. We confirmed downregulation of four more miRNAs selected at random (mir-299, mir-324-5p, mir-491, mir-532) by follow-up qRT-PCR analysis (**Supplementary Fig. 3**).

We used TargetScan (version 4)[39] and PicTar[40] to identify putative seed sites for all downregulated mature miRNAs within the 3′ UTR of all unique known GeneChip transcripts within the TargetScan or

Table 1 miRNAs downregulated in both PFC and hippocampus of *Df(16)A*$^{+/-}$ mice

	PFC		HPC					
miRNA (mmu-miR)	FDR *P*-value	Relative expression	FDR *P*-value	Relative expression	Chr.	Chr. start	Chr. end	Strand
185	3.6×10^{-8}	0.42	6.5×10^{-12}	0.41	16	18240964	18241028	–
134	2.2×10^{-4}	0.62	2.5×10^{-3}	0.57	12	110181946	110182016	+
674	2.2×10^{-4}	0.65	1.0×10^{-5}	0.75	2	116876568	116876667	+
532	3.3×10^{-4}	0.66	2.7×10^{-4}	0.61	X	6405361	6405456	–
673	6.6×10^{-4}	0.55	1.3×10^{-5}	0.64	12	110019797	110019887	+
674*	1.3×10^{-3}	0.68	1.4×10^{-5}	0.69	2	116876568	116876667	+
224	1.4×10^{-3}	0.27	1.4×10^{-3}	0.29	X	68513751	68513832	–
491	1.4×10^{-3}	0.60	1.4×10^{-3}	0.69	4	87593271	87593356	+
93	1.5×10^{-3}	0.83	2.9×10^{-3}	0.73	5	138395311	138395398	–
383	1.7×10^{-3}	0.75	6.9×10^{-3}	0.75	8	39720650	39720719	–
212	1.8×10^{-3}	0.77	1.2×10^{-4}	0.73	11	74989583	74989673	+
422b	3.1×10^{-3}	0.59	4.8×10^{-6}	0.54	18	61523204	61523269	–
708	4.1×10^{-3}	0.58	1.2×10^{-2}	0.67	12	110824290	110824356	+
540	4.1×10^{-3}	0.41	1.0×10^{-4}	0.53	7	96124616	96124724	+
106b	4.8×10^{-3}	0.80	4.0×10^{-3}	0.73	5	138395525	138395606	–
140*	6.1×10^{-3}	0.59	4.2×10^{-4}	0.67	8	110440373	110440442	+
194	6.1×10^{-3}	0.74	5.5×10^{-3}	0.74	1	187014107	187014173	+
194					19	6264643	6264728	+
325	6.1×10^{-3}	0.66	1.8×10^{-3}	0.73	X	101581801	101581898	–
494	6.1×10^{-3}	0.55	5.1×10^{-4}	0.58	12	110163125	110163209	+
362	7.5×10^{-3}	0.53	4.9×10^{-3}	0.67	X	6398941	6399005	–
409	1.7×10^{-2}	0.78	3.2×10^{-5}	0.78	12	110190965	110191043	+
323	1.7×10^{-2}	0.77	3.5×10^{-3}	0.81	12	110160315	110160400	+
669a	2.1×10^{-2}	0.67	1.1×10^{-2}	0.75	2	10394706	10394802	+
151	2.2×10^{-2}	0.78	4.5×10^{-5}	0.78	15	73082071	73082138	–
18	3.0×10^{-2}	0.70	4.4×10^{-3}	0.64	14	113925688	113925783	+

Chr., chromosome; mmu, *Mus musculus*. An asterisk following an miRNA name indicates the less predominant mature form when miRNA hairpin precursors give rise to two excised miRNAs, one from each arm (see miRNA Registry at miRBase). There are two chromosomal loci for mir-194, designated 194-1 and 194-2.

PicTar databases that were differentially expressed in the PFC or hippocampus. miRNAs can modulate transcript stability, and their downregulation is expected to result in upregulation of target genes. Consistent with this expectation, we found that a higher proportion of upregulated PFC and hippocampal transcripts contained one or more potential seed sites for any of the affected miRNAs, as compared to downregulated transcripts (TargetScan: PFC, 81/210 (39%) versus 69/500 (14%), $P = 1.5 \times 10^{-8}$; hippocampus, 128/325 (40%) versus 4/73 (6%), $P = 1.5 \times 10^{-5}$; PicTar: PFC, 72/210 (34%) versus 62/500 (12%), $P = 1.2 \times 10^{-11}$; hippocampus, 104/325 (32%) versus 6/73 (8%), $P = 4.2 \times 10^{-5}$). A frequency distribution of the putative miRNA seed sites (**Supplementary Fig. 4** online) showed that this enrichment was exclusively confined to upregulated transcripts containing two or more seed sites (~20% of the upregulated transcripts in either PFC or hippocampus), indicating possible convergent effects of the affected miRNAs in regulating the stability of individual transcripts.

Dgcr8 deficiency alters miRNA biogenesis in *Df(16)A*$^{+/-}$ mice

To examine the functional consequences of alterations in miRNA biogenesis, we generated *Dgcr8*-deficient mice using an embryonic stem (ES) cell line carrying a β-geo (fusion of β-galactosidase and neomycin transferase) gene trap inserted into intron 8 of the *Dgcr8* gene (**Fig. 4a–e**) (see also **Supplementary Note**). Homozygous mice die before birth (unpublished data), but heterozygous mice are produced at the expected rate, appear physically healthy and show normal gross brain morphology (**Fig. 4f,g**). Analysis of heterozygous mice confirmed that *Dgcr8* deficiency underlay the alterations in miRNA biogenesis observed in the *Df(16)A*$^{+/-}$ mice. qRT-PCR analysis indicated that the *Mirg* gene and six pri-miRNA forms that showed significant upregulation in *Df(16)A*$^{+/-}$ mice were also significantly upregulated in *Dgcr8*-deficient mice (**Fig. 4h**). In addition, of five mature miRNAs tested, *mir-134*, *mir-324-5p*, *mir-491* and *mir-532* showed a decrease in both PFC and hippocampus, and *mir-299* showed a decrease in PFC (**Fig. 4i,j**), a pattern identical to the one observed in the *Df(16)A*$^{+/-}$ mice.

Dgcr8 deficiency affects PPI and cognitive performance

We asked whether haploinsufficiency at the *Dgcr8* locus and the ensuing alterations in miRNA biogenesis contributed to the behavioral and cognitive deficits observed in the *Df(16)A*$^{+/-}$ mice. *Dgcr8* heterozygous mice showed normal activity in a novel open-field environment (**Fig. 5a**). However, *Dgcr8* heterozygous mice showed deficits in the PPI test (**Fig. 5b**). This deficit is restricted to the lower prepulse intensities, consistent with the observation that more than one gene within the *Df(16)A* modulate PPI[16,20–22], as well as with previous findings that genes contributing to PPI at low prepulse intensities may differ from the ones contributing to inhibition at higher ones[41]. In addition, there were no genotypic differences in the amplitude of the startle response at 120 dB (data not shown). In control experiments, we showed that the PPI deficit in the *Dgcr8*$^{+/-}$ mice was not due to reduced hearing sensitivity at low pulse intensities (see also **Supplementary Note** and **Supplementary Fig. 2**).

When examined in cognitive tests, *Dgcr8* heterozygous mice showed normal freezing in the contextual (**Fig. 5c**) and cued (**Fig. 5d**) fear-conditioning paradigms. However, when tested in the

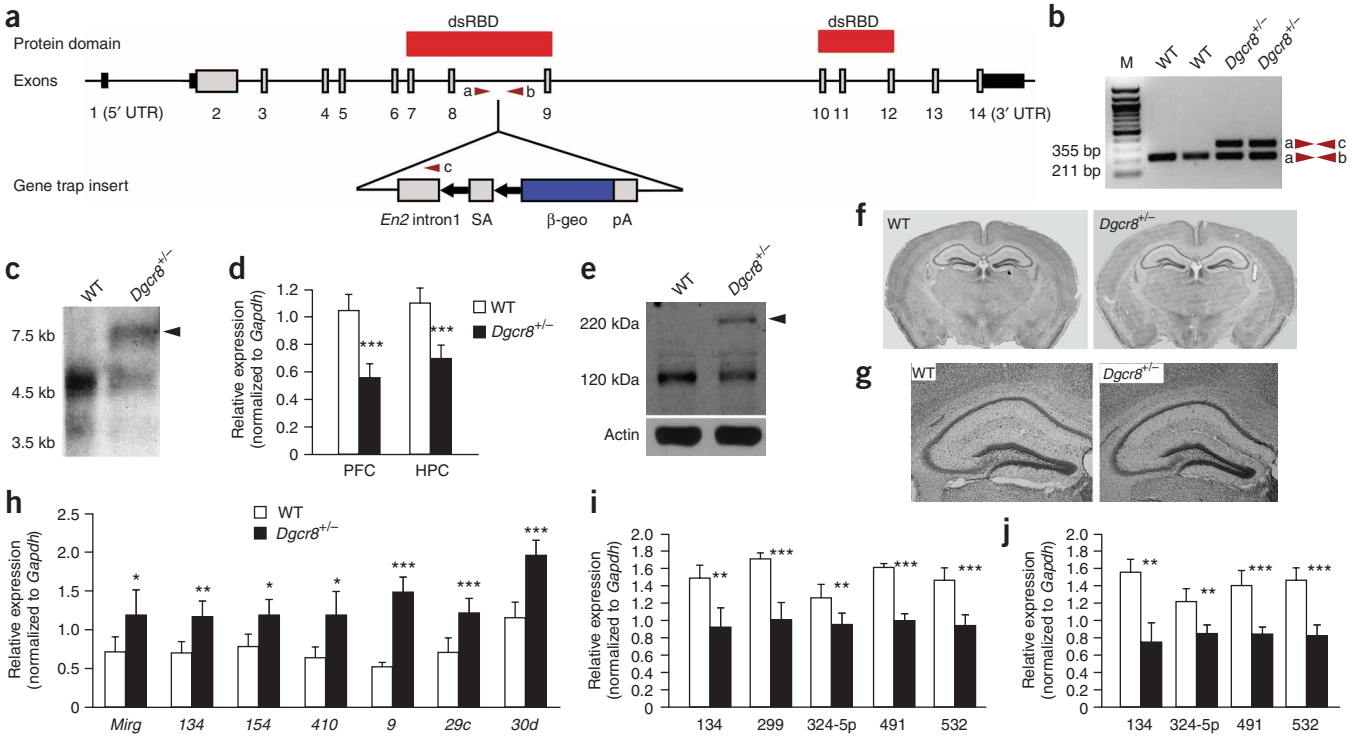

Figure 4 Production, validation and analysis of miRNA biogenesis in *Dgcr8*-deficient mice. (**a**) Diagram (not to scale) of genomic structure of *Dgcr8* and gene-trap insert in intron between exons 8 and 9. The two double-stranded RNA binding domains (dsRBD) of the protein are shown over the corresponding coding exons. *En2* intron 1, 1.5 kb of mouse *En2* intron 1; SA, splice acceptor of mouse *En2* exon 2; β-geo, fusion of β-galactosidase and neomycin transferase; pA, SV40 polyadenylation signal. Red arrowheads, approximate genomic location of PCR primers used for genotyping. (**b**) Results of PCR genotyping designed to verify the gene trap insertion in HET *Dgcr8*$^{+/-}$ mice. Arrowheads, primers shown in **a**. (**c**) RNA blot analysis showing reduced amount of WT 4.5-kb *Dgcr8* mRNA and production of the expected 7.2-kb chimeric mRNA (arrowhead) in *Dgcr8*$^{+/-}$ mice. (**d**) qRT-PCR analysis confirming reduction in WT *Dgcr8* mRNA in both PFC and hippocampus. Data are shown as mean ± s.e.m. (**e**) Protein blot analysis showing reduced amount of the 120-kDa WT Dgcr8 protein and production of the expected ~220-kDa chimeric protein product (arrowhead) in *Dgcr8*$^{+/-}$ mice. Actin was probed as a loading control. (**f**,**g**) Gross brain morphology of *Dgcr8*$^{+/-}$ mice by low-resolution histological examination of sections. Low magnification (**f**) and high magnification (**g**) images focused on the hippocampal region are shown. (**h**) qRT-PCR confirmation of the upregulation of the *Mirg* gene and six miRNA pri-forms in the PFC of the *Dgcr8*$^{+/-}$ mice. (**i**,**j**) qRT-PCR confirmation of the downregulation of five mature miRNAs tested in the PFC (**i**) and hippocampus (**j**) of *Dgcr8*$^{+/-}$ mice and WT littermate controls. $^{*}P < 0.05$, $^{**}P < 0.01$, $^{***}P < 0.001$. Data are shown as mean ± s.e.m.

cognitively more demanding spatial working memory–dependent learning task, *Dgcr8* heterozygous mice showed decreased arm choice accuracy ($P < 0.05$) over the course of the acquisition period (**Fig. 5e**), recapitulating the deficit observed in the *Df(16)A*$^{+/-}$ mice. Thus, our results suggest that haploinsufficiency at the *Dgcr8* locus and the ensuing impairment in miRNA processing contributes to the cognitive deficits induced by the *Df(16)A*$^{+/-}$ deficiency.

Dgcr8 deficiency affects dendritic spines and complexity

miRNAs may contribute to synaptic development and maturation[42], providing, at least in part, a potential explanation for the behavioral deficits observed in the *Dgcr8*$^{+/-}$ mice. Notably, analysis of spine morphogenesis *in vivo* in the CA1 subfield of the hippocampus of *Df(16)A*$^{+/-}$ mice revealed a reduction in the mushroom spine density (~25%, $P < 0.001$) and width (~10%, $P < 0.0001$), but not length. Decreases in density (but not size) of the dendritic spines could be accounted for, at least in part, by the deficiency of another gene residing in the deleted locus, *Zdhhc8* (Mukai *et al.*, unpublished data). Because altered dendritic spine development may underlie the observed behavioral deficits[43], we asked whether *Dgcr8* deficiency affected the density and morphology of dendritic spines *in vivo* by intercrossing the *Dgcr8*-deficient mice with a reporter strain (*Thy1-GFP/M* line) wherein CA1 hippocampal pyramidal neurons are intrinsically labeled in a relatively sparse mosaic manner with GFP throughout the cell body and dendritic tree[44]. Morphotypic analysis of mushroom spines showed that there was a significant decrease in the width of CA1 pyramidal spines (~8.5%, Kolmogorov-Smirnov test $P < 0.001$), whereas their length was unaffected (**Fig. 6a,b**), a pattern very similar to the one observed in the *Df(16)A*$^{+/-}$ mice. By contrast, we did not observe any changes in the mushroom spine density in the basal dendrites of CA1 pyramidal neurons from *Dgcr8*$^{+/-}$ mice compared to WT mice (*t*-test, $P > 0.05$) (**Fig. 6c**).

The effect of miRNAs on dendritic growth is unknown. Analysis of dendritic development *in vivo* in the CA1 subfield of the hippocampus of *Df(16)A*$^{+/-}$ mice showed a reduction in dendritic complexity of the basal dendritic tree of pyramidal neurons and a contribution of the *Zdhhc8* deficiency (Mukai *et al.*, unpublished data). We used compound heterozygous *Dgcr8*$^{+/-}$;*Thy1-GFP/M*$^{+/-}$ mice to ask whether *Dgcr8* deficiency affected the dendritic complexity at this hippocampus subfield. Sholl analysis (see Methods) indicated an overall genotype effect when comparing dendritic complexity at varying distances from the soma ($n = 30$, $P < 0.05$), primarily at the distal dendrites (**Fig. 6d,e**).

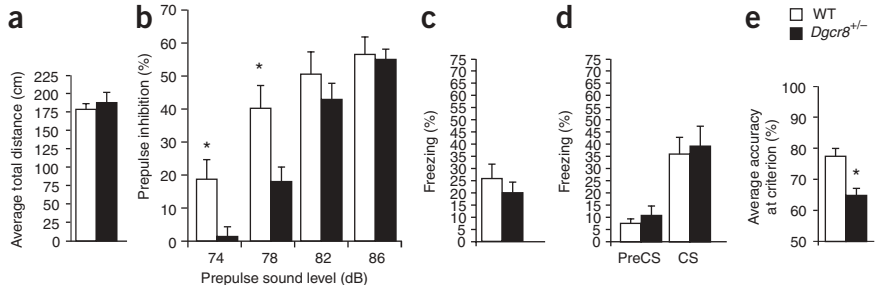

Figure 5 *Dgcr8* deficiency results in behavioral deficits. (**a**) Exploratory activity of *Dgcr8*$^{+/-}$ mice and WT littermate control mice in an open field. No significant difference was found in the total distance traveled in the open field between *Dgcr8*$^{+/-}$ mice and WT littermate control mice. (**b**) *Dgcr8*$^{+/-}$ mice showed impaired sensorimotor gating as assayed by the PPI test. Percent PPI was calculated as 100 – [(startle response of acoustic startle from acoustic prepulse and startle stimulus trials/startle response alone trials) × 100]. (**c**,**d**) Contextual (**c**) and cued (**d**) fear conditioning testing of *Dgcr8*$^{+/-}$ mice and WT littermate control mice. PreCS, preconditioned stimulus; CS, conditioned stimulus. (**e**) Spatial working memory–dependent learning test. *Dgcr8*$^{+/-}$ mice showed learning deficits, similar to the ones observed in *Df(16)A*$^{+/-}$ mice, in arm choice accuracy during the test acquisition period. *$P < 0.05$. Data are shown as mean ± s.e.m.

DISCUSSION

In the present study, we report results from our analysis of an engineered mouse strain (*Df(16)A*$^{+/-}$) carrying a hemizygous chromosomal deficiency that spans a segment of mouse chromosome 16 syntenic to the 1.5-Mb human 22q11 microdeletion[3], placing an emphasis on cognitive endophenotypes, as well as on linked molecular processes in relevant brain areas[45]. A fraction of *Df(16)A*$^{+/-}$ mice (~13%) die at birth, presumably from a number of cardiovascular abnormalities[23,24]. Milder forms of cardiac abnormalities were found to persist in only 18% of surviving adult mice of a similar strain[23] and therefore are unlikely to confound our analysis.

We provide evidence for an abnormality in brain miRNA processing emerging as a result of the downregulation of the *Dgcr8* gene. Our analysis showed that upon loss of one copy of the *Dgcr8* gene in the *Df(16)A*$^{+/-}$ mice, only a subset of pri-forms of miRNA genes was upregulated and a smaller subset of mature miRNAs was downregulated, a pattern that could not have been predicted from previous *in vitro* studies[36,46]. The end effect of *Dgcr8* haploinsufficiency was the downregulation of a specific subset of mature miRNAs identified by our miRNA profiling analysis. In most of the cases the expression of miRNAs was reduced by ~20–70%. Whether partial reduction in miRNA abundance within this range has an effect on transcript or protein levels of target genes has not been studied in a systematic manner, but it is strongly suggested by a recent study[47]. In addition, because target mRNAs can be simultaneously bound and repressed by more than one miRNA species in a manner that allows for cooperativity between target sites, the degree of repression achieved may be highly sensitive to the amount of available miRNA complexes and the number of the affected miRNAs[39,48]. Consistent with the expectation that synchronous modest decreases in several miRNAs may have considerable impact on target transcript stability, we showed that impaired miRNA biogenesis could account for at least a portion of the transcript upregulation observed in the PFC and hippocampus of the *Df(16)A*$^{+/-}$ mice. However, identification of the entire set of genuine mRNA targets *in vivo*, as well as elucidation of the effects of the observed miRNA downregulation on mRNA translation, will be the subject of future investigation. In addition, although DGCR8 may be the only member of the miRNA processing pathway that is specific to miRNAs[46], it remains to be determined whether reduction of miRNAs alone is the cause of the *Dgcr8* deficiency phenotype.

We showed that *Dgcr8* deficiency resulted in smaller dendritic spines and simpler dendritic tree and impaired sensorimotor gating and acquisition of a spatial working memory–dependent task. As we tested only male *Dgcr8*$^{+/-}$ mice, whether sexually dimorphic effects exist remains to be determined. Independent of the underlying mechanism, our finding highlights the functional consequences of

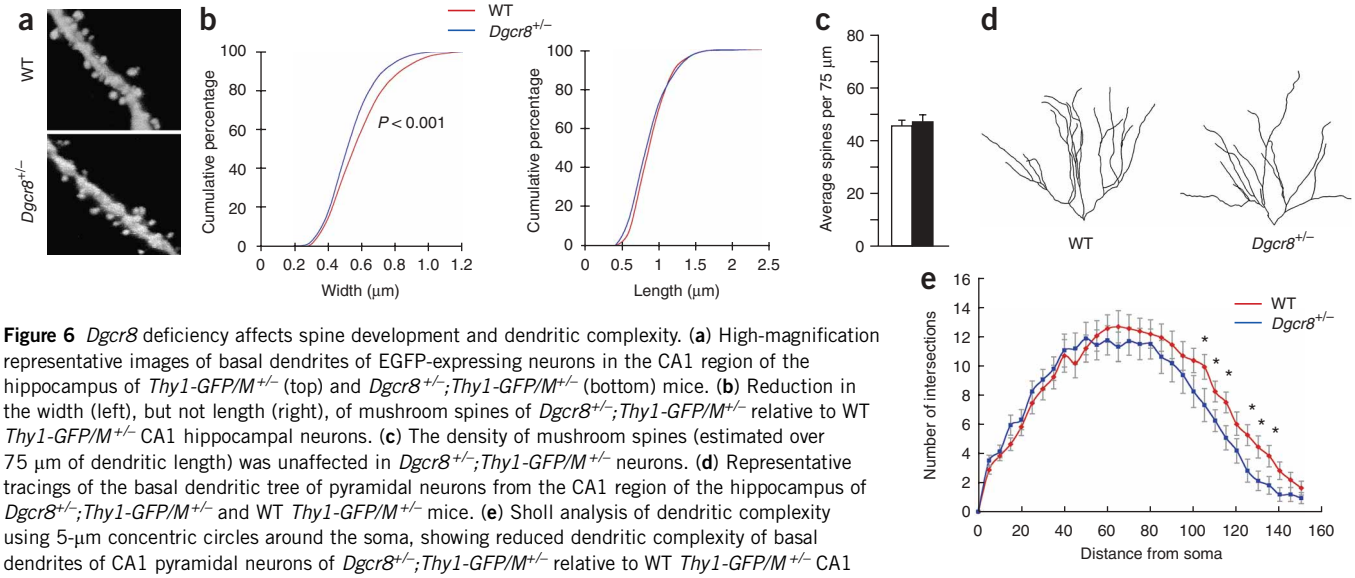

Figure 6 *Dgcr8* deficiency affects spine development and dendritic complexity. (**a**) High-magnification representative images of basal dendrites of EGFP-expressing neurons in the CA1 region of the hippocampus of *Thy1-GFP/M*$^{+/-}$ (top) and *Dgcr8*$^{+/-}$*;Thy1-GFP/M*$^{+/-}$ (bottom) mice. (**b**) Reduction in the width (left), but not length (right), of mushroom spines of *Dgcr8*$^{+/-}$*;Thy1-GFP/M*$^{+/-}$ relative to WT *Thy1-GFP/M*$^{+/-}$ CA1 hippocampal neurons. (**c**) The density of mushroom spines (estimated over 75 μm of dendritic length) was unaffected in *Dgcr8*$^{+/-}$*;Thy1-GFP/M*$^{+/-}$ neurons. (**d**) Representative tracings of the basal dendritic tree of pyramidal neurons from the CA1 region of the hippocampus of *Dgcr8*$^{+/-}$*;Thy1-GFP/M*$^{+/-}$ and WT *Thy1-GFP/M*$^{+/-}$ mice. (**e**) Sholl analysis of dendritic complexity using 5-μm concentric circles around the soma, showing reduced dendritic complexity of basal dendrites of CA1 pyramidal neurons of *Dgcr8*$^{+/-}$*;Thy1-GFP/M*$^{+/-}$ relative to WT *Thy1-GFP/M*$^{+/-}$ CA1 neurons. Branching appears normal toward the soma but is deficient at distances beyond 100 μm from the soma. *$P < 0.05$. Data are shown as mean ± s.e.m.

the observed reduction in miRNA abundance and implicates alterations in miRNA processing in understanding the basis of the synaptic and behavioral deficits of this mouse model and possibly of the human syndrome. We have previously shown that combined deficiency of two other genes in this locus (*Prodh* and *Comt*)[16] also affects working memory–based performance and dopamine neurotransmission. Combined deficiency of the same two genes[16], as well as two additional genes in this locus (*Tbx1*, *Gnbl1*)[22], has been previously shown to impair sensorimotor gating. In addition, complementary effects of *Dgcr8* and *Zdhhc8* deficiency seem to underlie the impaired dendritic growth and spine development observed in the *Df(16)A*$^{+/-}$ mice. Thus, *DGCR8* haploinsufficiency, although not solely responsible, is very likely to interact with haploinsufficiency of other 22q11.2 genes to produce the synaptic alterations as well as the cognitive and behavioral deficits associated with the 22q11.2 microdeletions.

To our knowledge, this is the first time that abnormal miRNA biogenesis has been shown to affect cognitive performance in mice. Notably, in male *Dgcr8*$^{+/-}$ mice, spatial working memory–based learning seemed to be primarily affected, whereas in male *Df(16)A*$^{+/-}$ mice associative learning was also compromised. The difference between the two cognitive tasks could be related to disparities in the underlying cognitive demands and the complexity of the relevant neural circuits, the differential sensitivity to disruptions of miRNA biogenesis, or the efficacy of compensatory mechanisms deployed as a result thereof. Along similar lines, it was recently shown that long-term memory in *Drosophila melanogaster* is regulated by components of the RISC complex[49]. Also, the fragile X syndrome–related protein FMRP regulates mRNA translation in the dendrites through association with RISC factors and miRNAs[50].

In summary, our results indicate that abnormal processing of miRNAs contributes to the behavioral and neuronal deficits associated with the human 22q11.2 microdeletion In addition, our findings could have more general implications for understanding the genetic basis of cognitive and psychiatric disorders. In particular, our results suggest that the potential of miRNAs to contribute to the regulation of expression of many genes in the brain[38] could be an important component of the genetically complex architecture of such disorders.

METHODS

Gene targeting and generation of *Df(16)A*$^{+/-}$ mice. We used chromosomal engineering[25] to generate mice with a 1.3-Mb heterozygous deletion on chromosome 16, as described in detail in **Supplementary Methods**. FISH is also described in detail in **Supplementary Methods**.

Generation of *Dgcr8*$^{+/-}$ mice. The XH157 ES cell line was obtained from BayGenomics (see URLs below). The gene-trap insert location was determined by using PCR followed by sequencing. ES clones were then amplified and injected into C57BL/6J blastocysts. Resulting chimeric males were bred to C57BL/6J females in order to obtain F_1 mice. PCR on DNA from tails followed by sequencing was used to confirm the presence of the gene-trap insertion. Once these mouse lines were confirmed, maintenance was performed by PCR genotyping. A common *Dgcr8*-specific forward PCR primer (*Dgcr8*-F), a *Dgcr8* specific reverse primer (*Dgcr8*-R) and a gene-trap–specific reverse primer (Gene trap-R) were used for *Dgcr8* genotyping (see **Supplementary Table 5** online for primers). The expected PCR product from the WT *Dgcr8* allele is 211 bp and the expected PCR product from the trapped *Dgcr8* allele is 355 bp. The mutation was backcrossed into the C57BL/6J background for three generations.

RNA isolation. RNA isolation for expression profiling was performed as described in **Supplementary Methods**.

Microarray data analysis. We analyzed initial microarray images obtained by our GeneChip (Affymetrix) analysis by using Microarray Suite version 5 (Affymetrix) to extract intensity values for each probe set. We then imported the .CEL files into ArrayAssist software (version 4.0, Stratagene). The raw data were first normalized by the GC Robust Multichip Average (GC-RMA) method implemented in ArrayAssist. Normalized data were then log transformed before any statistical analysis was conducted. Student's *t*-tests were used to identify genes that showed genotype-dependent differential expression. Benjamini and Hochberg FDR was used to control false positives due to multiple testing. The FDR was set at 0.01 unless indicated otherwise. Gene class testing and pathway analysis were performed as described in **Supplementary Methods**.

Identification of Affymetrix probe sets potentially assaying miRNA-containing primary transcripts. Probe sequences from the Affymetrix MOE430A (known target mRNAs) were aligned to the mm8 GoldenPath assembly of the mouse genome. The University of California Santa Cruz genome annotation database was used to identify genome alignments that overlapped regions containing miRNAs from miRBase (Sanger Institute; see URLs). Alignments were required to either directly overlap an miRBase miRNA location or overlap a potential transcript (based on RefSeq and mRNA information in the genome annotation database) that bridged the probe alignment with the miRNA location. Transcripts that had evidence from mRNAs were considered only if no RefSeq or 'known genes' were assigned to the probe alignment. This analysis yielded a set of 567 Affymetrix probe sets that potentially assayed at least one miRNA-containing transcript. The full list of these 'miRNA probe sets' is available upon request.

miRNA microarray expression analysis. We isolated 10 μg of total RNA from the PFCs and hippocampi of 8-week-old male mice using the mirVana miRNA isolation kit (Ambion). Small RNAs (<300 nt) were then isolated and processed for microarray analysis (LC Sciences). Briefly, purified small RNAs were labeled with Cy3 (WT) or Cy5 (*Df(16)A*$^{+/-}$) fluorescent dyes and hybridized to dual-channel microarray μParaFlo microfluidics chips (LC Sciences) containing 386 miRNA probes to mouse mature miRNAs. Each of the spotted detection probes consisted of a nucleotide sequence complementary to a specific miRNA sequence and a long non-nucleotide spacer that extended the specific sequence away from the chip surface. The miRNA probe sequences used were from the miRBase Sequence database version 9.1. We collected hybridization images using a GenePix 4000B laser scanner (Molecular Devices) and digitized them using Array-Pro image analysis software (Media Cybernetics). Raw data were imported in ArrayAssist 5.0 (Stratagene). The microarray data were corrected by removing spots with intensity equal to or below median background and then normalized with the LOWESS (locally weighted regression) method implemented in ArrayAssist 5.5 software (Stratagene). Differentiation analysis was conducted to determine the FDR *P*-value of each miRNA gene.

qRT-PCR. We performed qRT-PCR of the miRNA pri-forms and mature forms as described in detail in **Supplementary Methods**.

Behavioral phenotyping. We performed behavioral phenotyping as described in refs. 16 and 29, as well as in **Supplementary Methods**. We assessed behavioral performance identically in the two strains in open-field, spatial working memory and pavlovian fear conditioning tests (in that order). A different cohort was used in the PPI test. Two other cohorts of *Df(16)A*$^{+/-}$ mice were used to replicate the hyperactivity and the auditory cued conditioning phenotypes.

All mice were at least 8 weeks old at testing initiation. All animal procedures were performed according to protocols approved by the Columbia University Institutional Animal Care and Use Committee under federal and state regulations.

Analysis of spine morphology. *Dgcr8*$^{+/-}$ mice were crossed to the *Thy1-GFP/M* mouse line. Six *Dgcr8*$^{+/-}$;*Thy1-GFP/M*$^{+/-}$ and six WT *Thy1-GFP/M*$^{+/-}$ littermates, 8 weeks old, were perfused with 4% paraformaldehyde, their brains were dissected and 90-μm sections were generated using a vibratome (Leica). Hippocampal neuron images (CA1 subfield) were acquired on a Zeiss LSM5 510 laser-scanning confocal microscope. For each experiment, images across all genotypes were acquired with similar optimal settings for laser power, detector gain, and amplifier offset with a pinhole diameter equivalent to one Airy unit for the 488 nm laser. Twelve-bit images were obtained using a ×63 objective at a resolution of 2,048 × 2,048 pixels. Images were acquired as a *z*-stack, and a maximum intensity projection of each neuron was created from the *z*-stack

using 60–80 sections (0.14 μm per section). An experimenter unaware of the genotype performed all imaging and analysis. Quantification of spine density, length, and width was performed manually using LSM Image Browser (Zeiss) and ImageJ (see URLs). One or two basal dendrites, each at least 75 μm in length, were analyzed from each CA1 neuron. We analyzed at least three neurons for each animal. In total, we quantified 37 neurons (19 from *Dgcr8*$^{+/-}$ and 18 from WT mice) and 1,378 spines (681 from *Dgcr8*$^{+/-}$ and 697 from WT mice). The length of the entire spine (including head and neck) was measured as the distance of a straight line drawn from the junction of the spine with the dendritic shaft to the furthest tip of the spine head. Spine width was measured as the distance of a straight line drawn across the widest part of the spine head. Spine density was assessed by Student's *t*-test. Distributions of the length and width of mushroom spines were compared using the Kolmogorov-Smirnov test.

Analysis of dendritic complexity. We acquired hippocampal neuron images (CA1 subfield) as described in the previous paragraph using a ×40 objective at a resolution of 1,024 × 1,024 pixels. Images were acquired as a *z*-stack and a maximum intensity projection of each neuron was created from the *z*-stack using 120–160 sections (0.45 μm per section). An experimenter unaware of the genotype performed all imaging and analysis. The raw projected 2D images were imported into ImageJ. The basal dendrite branches were traced from the somata of CA1 neurons using NeuronJ. The tracing images were then analyzed using Sholl Analysis Plugin (see URLs) with a 'radius step size' of 5 μm. The points where the dendrites crossed the lines of concentric rings were taken as intersecting points. We counted the number of dendritic branching points and intersections in successive radial segments of 5 μm by considering the center of the soma as a reference point.

URLs. BayGenomics, http://baygenomics.ucsf.edu/; miRBase, http://microrna.sanger.ac.uk/; ImageJ, http://rsb.info.nih.gov/ij/; Sholl Analysis Plugin, http://biology.ucsd.edu/labs/ghosh/software/; ErmineJ, http://www.bioinformatics.ubc.ca/ermineJ/.

Accession numbers. Gene Expression Omnibus: GSE10784.

Note: Supplementary information is available on the Nature Genetics website.

ACKNOWLEDGMENTS

We thank A. Merién for assistance with the dendritic complexity and spine analysis. We thank A. Abrams-Downey, C. Frazier, J. Pellegrino, D. Swor, Y. Sun and M. Sribour for technical support and assistance with the mouse colony. We also thank P.A. Arguello for help and insights with the behavioral assays. This research was supported in part by the US National Institutes of Health (grants MH067068 to M.K. and J.A.G. and MH077235 to J.A.G.) and the New York Academy of Sciences (J.A.G.). Support was also provided in part by a McKnight Brain Disorders award (J.A.G.) and a NARSAD award (J.A.G.), as well as an EJLB grant award (J.A.G.).

AUTHOR CONTRIBUTIONS

K.L.S., A.B., H.L. and A.A.M. contributed to the generation of the *Df16(A)*$^{+/-}$ line; K.L.S., B.X. and W.-S.L. performed the behavioral assays; B.X. and R.H. contributed to the generation and validation of the *Dgcr8*$^{+/-}$ line; B.X. performed the mRNA and miRNA expression analysis and the dendritic spine and complexity analysis; X.W. and P.P. contributed to the bioinformatic analysis of the mRNA expression data; M.K. and J.A.G. contributed to the research design and supervised the project.

Published online at http://www.nature.com/naturegenetics
Reprints and permissions information is available online at http://npg.nature.com/reprintsandpermissions

1. Botto, L.D. *et al.* A population-based study of the 22q11.2 deletion: phenotype, incidence, and contribution to major birth defects in the population. *Pediatrics* **112**, 101–107 (2003).
2. McDonald-McGinn, D.M. *et al.* Phenotype of the 22q11.2 deletion in individuals identified through an affected relative: cast a wide FISHing net!. *Genet. Med.* **3**, 23–29 (2001).
3. Edelmann, L., Pandita, R.K. & Morrow, B.E. Low-copy repeats mediate the common 3-Mb deletion in patients with velo-cardio-facial syndrome. *Am. J. Hum. Genet.* **64**, 1076–1086 (1999).
4. Woodin, M. *et al.* Neuropsychological profile of children and adolescents with the 22q11.2 microdeletion. *Genet. Med.* **3**, 34–39 (2001).
5. Gothelf, D. *et al.* Genetic, developmental, and physical factors associated with attention deficit hyperactivity disorder in patients with velocardiofacial syndrome. *Am. J. Med. Genet. B. Neuropsychiatr. Genet.* **126**, 116–121 (2004).
6. Gothelf, D. *et al.* Obsessive-compulsive disorder in patients with velocardiofacial (22q11 deletion) syndrome. *Am. J. Med. Genet. B. Neuropsychiatr. Genet.* **126**, 99–105 (2004).
7. Marshall, C.R. *et al.* Structural variation of chromosomes in autism spectrum disorder. *Am. J. Hum. Genet.* **82**, 477–488 (2008).
8. Green, M.F. *et al.* Approaching a consensus cognitive battery for clinical trials in schizophrenia: the NIMH-MATRICS conference to select cognitive domains and test criteria. *Biol. Psychiatry* **56**, 301–307 (2004).
9. Sobin, C. *et al.* Neuropsychological characteristics of children with the 22q11 deletion syndrome: a descriptive analysis. *Child Neuropsychol.* **11**, 39–53 (2005).
10. Pulver, A.E. *et al.* Psychotic illness in patients diagnosed with velo-cardio-facial syndrome and their relatives. *J. Nerv. Ment. Dis.* **182**, 476–478 (1994).
11. Karayiorgou, M. *et al.* Schizophrenia susceptibility associated with interstitial deletions of chromosome 22q11. *Proc. Natl. Acad. Sci. USA* **92**, 7612–7616 (1995).
12. Gothelf, D. *et al. COMT* genotype predicts longitudinal cognitive decline and psychosis in 22q11.2 deletion syndrome. *Nat. Neurosci.* **8**, 1500–1502 (2005).
13. Liu, H. *et al.* Genetic variation in the 22q11 locus and susceptibility to schizophrenia. *Proc. Natl. Acad. Sci. USA* **99**, 16859–16864 (2002).
14. Liu, H. *et al.* Genetic variation at the 22q11 *PRODH2/DGCR6* locus presents an unusual pattern and increases susceptibility to schizophrenia. *Proc. Natl. Acad. Sci. USA* **99**, 3717–3722 (2002).
15. Mukai, J. *et al.* Evidence that the gene encoding ZDHHC8 contributes to the risk of schizophrenia. *Nat. Genet.* **36**, 725–731 (2004).
16. Paterlini, M. *et al.* Transcriptional and behavioral interaction between 22q11.2 orthologs modulates schizophrenia-related phenotypes in mice. *Nat. Neurosci.* **8**, 1586–1594 (2005).
17. Raux, G. *et al.* Involvement of hyperprolinemia in cognitive and psychiatric features of the 22q11 deletion syndrome. *Hum. Mol. Genet.* **16**, 83–91 (2007).
18. Williams, N.M. *et al.* Strong evidence that *GNB1L* is associated with schizophrenia. *Hum. Mol. Genet.* **17**, 555–566 (2008).
19. Swerdlow, N.R., Geyer, M.A. & Braff, D.L. Neural circuit regulation of prepulse inhibition of startle in the rat: current knowledge and future challenges. *Psychopharmacology (Berl.)* **156**, 194–215 (2001).
20. Gogos, J.A. *et al.* The gene encoding proline dehydrogenase modulates sensorimotor gating in mice. *Nat. Genet.* **21**, 434–439 (1999).
21. Kimber, W.L. *et al.* Deletion of 150 kb in the minimal DiGeorge/velocardiofacial syndrome critical region in mouse. *Hum. Mol. Genet.* **8**, 2229–2237 (1999).
22. Paylor, R. *et al. Tbx1* haploinsufficiency is linked to behavioral disorders in mice and humans: implications for 22q11 deletion syndrome. *Proc. Natl. Acad. Sci. USA* **103**, 7729–7734 (2006).
23. Lindsay, E.A. *et al.* Congenital heart disease in mice deficient for the DiGeorge syndrome region. *Nature* **401**, 379–383 (1999).
24. Merscher, S. *et al. TBX1* is responsible for cardiovascular defects in velo-cardio-facial/DiGeorge syndrome. *Cell* **104**, 619–629 (2001).
25. Zheng, B., Mills, A.A. & Bradley, A. A system for rapid generation of coat color-tagged knockouts and defined chromosomal rearrangements in mice. *Nucleic Acids Res.* **27**, 2354–2360 (1999).
26. Long, J.M. *et al.* Behavior of mice with mutations in the conserved region deleted in velocardiofacial/DiGeorge syndrome. *Neurogenetics* **7**, 247–257 (2006).
27. Paylor, R. *et al.* Mice deleted for the DiGeorge/velocardiofacial syndrome region show abnormal sensorimotor gating and learning and memory impairments. *Hum. Mol. Genet.* **10**, 2645–2650 (2001).
28. Phillips, R.G. & LeDoux, J.E. Differential contribution of amygdala and hippocampus to cued and contextual fear conditioning. *Behav. Neurosci.* **106**, 274–285 (1992).
29. Koike, H., Arguello, P.A., Kvajo, M., Karayiorgou, M. & Gogos, J.A. *Disc1* is mutated in the 129S6/SvEv strain and modulates working memory in mice. *Proc. Natl. Acad. Sci. USA* **103**, 3693–3697 (2006).
30. Jones, M.W. & Wilson, M.A. Theta rhythms coordinate hippocampal-prefrontal interactions in a spatial memory task. *PLoS Biol.* **3**, e402 (2005).
31. Kellendonk, C. *et al.* Transient and selective overexpression of dopamine D2 receptors in the striatum causes persistent abnormalities in prefrontal cortex functioning. *Neuron* **49**, 603–615 (2006).
32. Jurata, L.W. *et al.* Altered expression of hippocampal dentate granule neuron genes in a mouse model of human 22q11 deletion syndrome. *Schizophr. Res.* **88**, 251–259 (2006).
33. Meechan, D. *et al.* Gene dosage in the developing and adult brain in a mouse model of 22q11 deletion syndrome. *Mol. Cell. Neurosci.* **33**, 412–428 (2006).
34. Sivagnanasundaram, S. *et al.* Differential gene expression in the hippocampus of the Df1/+ mice: a model for 22q11.2 deletion syndrome and schizophrenia. *Brain Res.* **1139**, 48–59 (2007).
35. Seitz, H. *et al.* A large imprinted microRNA gene cluster at the mouse Dlk1-Gtl2 domain. *Genome Res.* **14**, 1741–1748 (2004).
36. Tomari, Y. & Zamore, P.D. MicroRNA biogenesis: drosha can't cut it without a partner. *Curr. Biol.* **15**, R61–R64 (2005).
37. Wheeler, G., Ntounia-Fousara, S., Granda, B., Rathjen, T. & Dalmay, T. Identification of new central nervous system specific mouse microRNAs. *FEBS Lett.* **580**, 2195–2200 (2006).
38. Kosik, K.S. The neuronal microRNA system. *Nat. Rev. Neurosci.* **7**, 911–920 (2006).
39. Lewis, B.P., Shih, I.H., Jones-Rhoades, M.W., Bartel, D.P. & Burge, C.B. Prediction of mammalian microRNA targets. *Cell* **115**, 787–798 (2003).

40. Krek, A. *et al.* Combinatorial microRNA target predictions. *Nat. Genet.* **37**, 495–500 (2005).
41. Paylor, R. & Crawley, J.N. Inbred strain differences in prepulse inhibition of the mouse startle response. *Psychopharmacology (Berl.)* **132**, 169–180 (1997).
42. Schratt, G.M. *et al.* A brain-specific microRNA regulates dendritic spine development. *Nature* **439**, 283–289 erratum **441**, 902 (2006).
43. Feng, G. *et al.* Imaging neuronal subsets in transgenic mice expressing multiple spectral variants of GFP. *Neuron* **28**, 41–51 (2000).
44. Matsuzaki, M., Honkura, N., Ellis-Davies, G.C. & Kasai, H. Structural basis of long-term potentiation in single dendritic spines. *Nature* **429**, 761–766 (2004).
45. Arguello, P.A. & Gogos, J.A. Modeling madness in mice: one piece at a time. *Neuron* **52**, 179–196 (2006).
46. Wang, Y., Medvid, R., Melton, C., Jaenisch, R. & Blelloch, R. DGCR8 is essential for microRNA biogenesis and silencing of embryonic stem cell self-renewal. *Nat. Genet.* **39**, 380–385 (2007).
47. Zhao, Y. *et al.* Dysregulation of cardiogenesis, cardiac conduction, and cell cycle in mice lacking miRNA-1–2. *Cell* **129**, 303–317 (2007).
48. Doench, J.G., Petersen, C.P. & Sharp, P.A. siRNAs can function as miRNAs. *Genes Dev.* **17**, 438–442 (2003).
49. Ashraf, S.I., McLoon, A.L., Sclarsic, S.M. & Kunes, S. Synaptic protein synthesis associated with memory is regulated by the RISC pathway in *Drosophila*. *Cell* **124**, 191–205 (2006).
50. Caudy, A.A., Myers, M., Hannon, G.J. & Hammond, S.M. Fragile X-related protein and VIG associate with the RNA interference machinery. *Genes Dev.* **16**, 2491–2496 (2002).